

InvertAvatar: Incremental GAN Inversion for Generalized Head Avatars

Xiaochen Zhao^{1*}, Jingxiang Sun^{1*}, Lizhen Wang¹, Yebin Liu¹

¹Department of Automation, Tsinghua University



Figure 1. Given single or more source images, our method rapidly reconstructs photorealistic 3D facial avatars under one second, enabling precise control over full-head rotations and subtle expressions like lopsided grins and eye gazes.

Abstract

While high fidelity and efficiency are central to the creation of digital head avatars, recent methods relying on 2D or 3D generative models often experience limitations such as shape distortion, expression inaccuracy, and identity flickering. Additionally, existing one-shot inversion techniques fail to fully leverage multiple input images for detailed feature extraction. We propose a novel framework, **Incremental 3D GAN Inversion**, that enhances avatar reconstruction performance using an algorithm designed to increase the fidelity from multiple frames, resulting in improved reconstruction quality proportional to frame count. Our method introduces a unique animatable 3D GAN prior with two crucial modifications for enhanced expression controllability alongside an innovative neural texture en-

coder that categorizes texture feature spaces based on UV parameterization. Differentiating from traditional techniques, our architecture emphasizes pixel-aligned image-to-image translation, mitigating the need to learn correspondences between observation and canonical spaces. Furthermore, we incorporate ConvGRU-based recurrent networks for temporal data aggregation from multiple frames, boosting geometry and texture detail reconstruction. The proposed paradigm demonstrates state-of-the-art performance on one-shot and few-shot avatar animation tasks.

1. Introduction

The creation of digital head avatars [3, 11, 13, 16, 19, 35, 48, 57, 59, 60] has long been a task of interest in the fields of computer vision and graphics. The ability to interactively generate photo-realistic head avatars opens up new possi-

*Equal Contribution

bilities in areas such as augmented/virtual reality (AR/VR), 3D telepresence, and video conferencing. The primary aims when developing a digital head avatar are two-fold: high fidelity and efficiency. High fidelity involves preserving intricate details from input images, reconstructing occluded facial regions (especially in profile views), and accurately modeling dynamic features such as facial expressions, all while maintaining consistent identity throughout animation. Efficiency demands a model that can adapt to varied unseen identities and motions without additional optimization at the inference stage.

Recent literature showcases numerous attempts to create avatars from a single input image and perform animation with video frames. Several 2D generative models [11, 13, 35, 48] perform image animation by incorporating the 3D Morphable Face Models (3DMM) [7] into the portrait synthesis. These 2D-based methods achieve photorealism but suffer from shape distortion during large motion due to a lack of geometry constraints.

Towards better view consistency, many recent efforts [4, 31] leverage 3D GAN prior and decouple motion and appearance in latent space with video data. The main drawback of this paradigm is that the motion and appearance are naturally entangled in 3D GAN which leads to expression inaccuracy and identity flickering during animation. The other line of works [29, 40, 41, 51] directly learn a controllable 3D GAN from only 2D image collections, and perform GAN inversion to restore an avatar from one single image. The methods employing the controllable generative prior demonstrate efficiency, yet they are constrained by their dependency on a singular source image. A single image often falls short in fully representing the subject owing to factors such as occlusions and limited pose information. Utilizing diverse source images enriches appearance data, thereby diminishing the extent of hallucination required by an image generator. However, these one-shot inversion techniques do not directly enable the aggregation of partial observations across distinct frames to reconstruct more personalized details. Consequently, this represents a significant limitation to their capacity for detailed feature extraction.

In this paper, we address the challenge of enhancing avatar reconstruction performance when multiple input images are present. Our proposed algorithm is designed to elevate the fidelity of the recovered avatar both within and beyond the face region across multiple frames, with improvements in personal detail reconstruction scaling with the increase in frame count. To achieve this, we introduce a novel framework capable of efficient incremental 3D head avatar reconstruction, fusing multiple inputs without necessitating any additional optimization during inference from a sequence of monocular images.

Specifically, we utilize an animatable 3D GAN prior, incorporating two key modifications to enhance expression

controllability’s efficiency and accuracy. Subsequently, we introduce an innovative neural texture encoder designed to categorize texture feature spaces in accordance with UV parameterization. This differentiates our approach from prevalent techniques that depend on networks to map an unposed image to a canonical tri-plane representation. Our proposed architecture emphasizes pixel-aligned image-to-image translation, which effectively eradicates the need for learning correspondences between observation and canonical spaces. This focus significantly improves its capacity for recovering fine details.

To accumulate temporal data from numerous frames, we further modify the one-shot inversion architecture to accommodate multiple inputs by leveraging ConvGRU-based [5] recurrent networks. This unique recurrent mechanism allows a flexible number of inputs and autonomously determines which information should be retained or discarded within streaming frames, thereby bolstering geometry and texture detail reconstruction capabilities.

To summarize, the contributions of our approach are:

- We provide a new paradigm for efficient avatar reconstruction for streaming data based on a concept called incremental 3D GAN inversion. The paradigm supports one to multiple source images inputs and achieves state-of-the-art performance on one-shot and few-shot facial avatar animation tasks.
- We propose an innovative neural texture encoder alongside an animatable 3D GAN prior, allowing for the definition of a texture feature space on the UV parameterization which enhances the recovery of fine details by pixel-aligned nature.
- We incorporate recurrent Networks for temporal aggregation from multiple input frames extracted from monocular video, enhancing the quality of avatar reconstruction by considering sequential data.

2. Related Works

2.1. 3D GAN inversion

Building upon the achievements of 2D Generative Adversarial Network (GAN) inversion for image editing and manipulation [2, 12, 36, 45, 49], current 3D GAN inversion methodologies [26, 30, 39] perform a projection of specific images onto multiple instances within the pre-trained StyleGAN2 latent space [1, 23]. While the global latent space enhances 3D-aware portrait editing abilities, it results in a trade-off between reconstruction accuracy and editability, thereby complicating the accurate reconstruction of input images. Consequently, contemporary 3D GAN inversion techniques necessitate an estimated camera pose and slight generator weight adjustment [14, 37, 52] during testing to reconstruct out-of-domain input images accurately. In contrast to latent code inversion or tedious generator fine-

tuning, recent efforts have shifted towards directly applying 3D GAN inversion on a triplane architecture for 3D GANs. For instance, TriPlaneNet [6] presents a triplane encoder while Live3DPortrait [46] integrates a Vision Transformer architecture into the triplane encoder, both showing substantial enhancements in robustness and 3D inversion quality for out-of-domain images. Furthermore, Control3Diff [20] suggests a diffusion-based tri-plane encoder that demonstrates multimodal control capabilities.

2.2. 2D Facial animation with 3DMM

Blanz et al. [7] pioneered the modeling of facial texture and shape in vector spaces, leading to the development of the 3D Morphable Model (3DMM). Subsequent extensions of the 3DMM concept include full-head PCA models [9, 34] and blend-shape models [28], which have been extensively studied and widely implemented in facial animation tasks [18, 43]. While these methods leverage the benefits of 3DMM to accurately and continuously model facial part deformations, they grapple with representing non-facial areas that are beyond the scope of 3DMM, such as hair, teeth, eyes, and body. These methods also tend to lack fine-grained facial details. To compensate for these limitations and generate more realistic facial details, subsequent research [11, 13, 15, 17, 25, 35, 42, 44, 48, 54] has applied learned techniques atop 3DMM renderings. For instance, DiscoFaceGAN [11] maps 3DMM parameters into a latent space, subsequently decoupling them through imitative-contrastive learning. While these 2D-based approaches have successfully facilitated efficient and photorealistic animation, they do not model 3D geometry and hence fail to maintain stringent 3D consistency during significant head pose alterations.

2.3. Neural 3D head avatars

For strict 3D consistency, recent efforts [3, 16, 19, 57, 59] incorporate 3DMM into volumetric representations [21, 32, 33, 38] to achieve view-consistent facial animation. Although these methods demonstrate realistic reconstruction results, they inefficiently learn separate networks for different identities and require thousands of frames from a specific individual for training. Another line of works [4, 29, 31, 40, 56] focus on reconstructing 3D portraits in one-shot or few-shot manner incorporating 3D GAN prior or training in a generative manner. Next3D [40] learns a controllable 3D head avatar from random noise and reconstructs an avatar by PTI inversion. Li et al. [29] proposes to encode input images into a canonical branch for coarse geometry and texture, and introduces an additional appearance branch that captures personal details and an expression branch that modifies the reconstruction to the desired expression. These methods show efficient promising one-shot reconstruction but none of them are architected to accommodate the uti-

lization of multiple source images as input. Contrastingly, our proposed framework is designed to leverage the complementary information inherent in multiple input images, thereby facilitating superior reconstruction quality.

3. Method

Our method innovatively harnesses the prior knowledge embedded in an animatable 3D generative model, integrating it with an incremental inversion architecture to enable rapid and high-fidelity 3D avatar reconstruction. Utilizing either a single source image or a short sequence of dynamic frames from a source video, our system is capable of reconstructing a 3D facial avatar, which is readily animatable through a 3D Morphable Face Model (3DMM) [47]. In Sec. 3.1, we introduce our compact yet highly expressive animatable GAN, which provides a strong 3D prior. Sec. 3.2 details our one-shot learning-based avatar reconstruction method, intricately designed to capitalize on the aforementioned GAN prior. Conclusively, in Section 3.3, we describe the employment of RNN-based temporal aggregation networks, which are instrumental in enhancing the shape and appearance precision of the reconstructed avatar by harnessing temporal data.

3.1. Compact and Expressive Animatable 3D GAN

Drawing from Next3D [40] for our 3D facial avatar generator, we identified its drawbacks that restrict wider usability. Its complexity and numerous network parameters complicate inversion-friendly feature space creation, lead to high memory overhead, limit neural rendering resolution, and introduce view inconsistency. It also struggles with accurate animation according to the FLAME model. To address these, we proposed two key architectural changes enhancing animation precision and view consistency, reducing model size by half while retaining synthesis quality.

Compact face synthesis module. Next3D transforms neural texture into orthogonal views and forms tri-plane features. To compensate for the FLAME model’s missing inner mouth area, Next3D utilizes a UNet to supplement and reintegrate this texture, using another UNet for post-blending. These operations are redundant and lead to heavy parameter size, so we alternately propose a more compact architecture, maintaining the insight of completing inner mouth feature conditioning on global information, but removing heavy networks for specific mouth synthesis. Specifically, we propose a face synthesis module G_{face} , which is conditioned on the multi-scale rasterized neural textures. The multi-scale neural textures are rasterized from texture space into tri-plane space and then integrated with G_{face} ’s corresponding feature maps through alpha blending. Conditioned on such global information, G_{face} is precisely controlled by the deformable mesh model, and gradually inpaint inner mouth features in the forward pass layer by

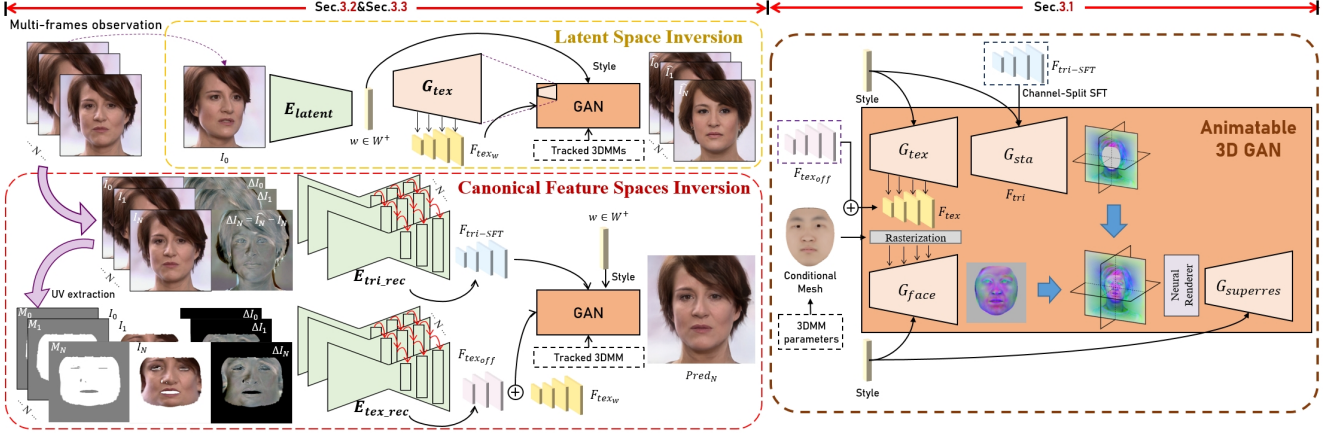


Figure 2. Our avatar reconstruction pipeline, applicable to a single or multi-image sequence, comprises two stages. The coarse stage inverts the first frame in the GAN prior’s $W+$ latent space with E_{latent} , forming an initial avatar. The fine stage employs recurrent networks $E_{tex.rec}$ and $E_{tri.rec}$ to aggregate temporal information, incrementally refining a high-fidelity avatar in two canonical feature spaces. The architecture of our advanced animatable 3D generative model is depicted in the right box.

layer. Additionally, our more memory-efficient and compact model design allows for neural rendering resolution of 128^2 , significantly enhancing view-consistency.

More expressive facial parametric model. The expressiveness of the facial parametric model is paramount for aligning the conditional morphable model with synthesized images. A misalignment between 3DMM and 2D image expressions can weaken their correlation during adversarial training, impeding the correct deformation of generated images. To rectify this, we employ Faceverse [47], a more expressive parametric model than the FLAME model [27]. With its extensive shape and expression bases, Faceverse accurately fits subtle expression changes in 2D images. During training, supplying the discriminator with the tracked landmarks map bolsters the consistency between synthesized images and the conditional mesh.

In the subsequent inversion and animation phases, we will initially fit Faceverse to the source portrait image or images of a person, capturing their expressions and head poses. Next, GAN inversion will be applied to reconstruct the corresponding head character. Finally, by changing the input expression parameters of FaceVerse, we gain the ability to animate the inverted avatar.

3.2. One-shot Avatar Reconstruction

To extract maximum personal information from a single image with the reconstructed avatar, we introduce an effective one-shot 3D GAN inversion framework. This framework utilizes a two-stage coarse-to-fine inversion architecture that carries out inversions in the latent and feature spaces of our animatable generative model separately. Due to the disentangled nature of the dynamic face and static head features, we divide the feature space into two specific

canonical spaces: F_{tex} defined by G_{tex} (the canonical texture space), and F_{tri} defined by G_{static} (the canonical tri-plane space). The ultimate goal then becomes learning the mapping from the input portrait image to the facial avatar represented in these latent and canonical feature spaces.

In the coarse stage, we introduce a latent encoder E_{latent} to project the image to the $W+$ latent space of the pretrained GAN. Specifically, given a source image I , we embed an inverted latent code $\hat{w} = E_{latent}(I)$ and initially generate a coarse facial avatar, represented by canonical features $F_{tex_w} = G_{tex}(\hat{w})$ and $F_{tri_w} = G_{static}(\hat{w})$. With the estimated pose and expression of the source image I , we can synthesize the fake image $\hat{I} = R(G_{face}(F_{tex_w}), F_{tri_w})$, where R is the rendering block.

In the second stage, with the aim to offset the information loss instigated by E_{latent} , we formulate two separate image encoders E_{tex} and E_{tri} . These are specifically designed to refine the feature maps in each of the two canonical spaces independently. Different from existing methods that rely on networks to map a posed image to the canonical tri-plane representation, benefiting from the neural texture architecture of our GAN prior, the face appearance represented by texture feature space is explicitly defined on the UV parameterization. Hence we design a U-Net network E_{tex} to translate the observation to the canonical texture feature space in the UV domain, as shown in Fig. 2. Such a pixel-aligned image-to-image translation architecture helps eliminate the learning burden of correspondences between observation space and canonical space, making it concentrate on recovering fine details, as demonstrated in Sec. 4.3.2. Specifically, the input of the E_{tex} contains three maps, the source image I and the residual map $\Delta I = I - \hat{I}$ that are projected to the UV plane, and a mask indicating the

visibility region of the face. E_{tex} outputs multi-resolution feature offsets $F_{tex_{off}}$ to compensate for the texture features F_{tex_w} obtained in the first stage.

As for the static tri-plane features, we introduce an image-to-plane encoder E_{tri} to predict multi-scale feature maps. Specifically, the multi-resolution features $F_{tri-SFT}$ output by E_{tri} are used to spatially modulate G_{static} with the CS-SFT layer [50] in a coarse-to-fine manner.

The training for all image encoders can also be divided into two stages. Firstly, we only train E_{latent} , with the loss terms following [36, 45]. Secondly, we simultaneously train E_{tex} and E_{tri} . Referring to Live 3D Portrait [46], our training set includes the synthetic data and we supervise the training with many intermediate feature maps, as well as an adversarial loss to generate photo-realistic results. Please refer to our supplemental material for more details.

3.3. Incremental GAN inversion

While the aforementioned GAN encoder effectively facilitates high-quality one-shot avatar reconstruction, a solitary image lacks sufficient pose and expression information to fully portray the shape and appearance. Therefore, we propose an approach termed *Incremental GAN Inversion*: incrementally enhances the quality of GAN inversion while concurrently integrating temporal information.

We transition from a one-shot to a multi-frame inversion structure using temporal aggregation networks $E_{tex.rec}$ and $E_{tri.rec}$ equipped with recurrent decoders. Given an input video clip $\mathbf{I}^N = \{I_t\}_0^N$, we aim at fusing the information of all frames to generate canonical representation F_{tex} and F_{tri} . First, the first frame is input to the E_{latent} for $W+$ space latent code w and initial canonical features F_{tex_w} and F_{tri_w} . According to the poses and expressions of the input sequence, we synthesize a fake image sequence and calculate the residual map for each frame $\Delta I_t = I_t - \hat{I}_t$. We sequentially input the observation and residual of each frame into the network $E_{tex.rec}$ and $E_{tri.tex}$ respectively on the UV domain and the picture domain.

Performing in a seq2one fashion, the recurrent decoders of $E_{tex.rec}$ and $E_{tri.tex}$ merge frame-wise feature maps in the temporal domain to predict one $F_{tri-SFT}$ and $F_{tex_{off}}$. Specifically, the recurrent decoder adopts ConvGRU [5] at each scale to aggregate temporal information, which is defined as:

$$\begin{aligned} z_t, r_t &= \sigma(\text{Conv}(f_t, h_{t-1})) \\ o_t &= \tanh(\text{Conv}(f_t, r_t * h_{t-1})) \\ h_t &= z_t * h_{t-1} + (1 - z_t) * o_t \end{aligned} \quad (1)$$

where operator $*$ denotes element-wise product. For each ConvGRU block, the feature map of one frame f_t is input to calculate the update weights map z_t and reset weights map r_t , to merge the current frame’s information into hidden state h_t . With the initial recurrent state h_0 all zero ten-

sor, after inputting all frames in turn, the final fully updated hidden state serves as the output.

Contrary to systems employing straightforward feed forwarding of multiple frames as auxiliary inputs, our recurrent mechanism accommodates a flexible number of inputs. It intelligently learns the information to keep or discard from streaming data, thereby circumventing the constraints of fixed-size input windows and interval-based updates.

4. Experiments

4.1. Experiment Setting

Baseline methods. We mainly compare our method with image-driven-based generalized head avatar reenactment methods, including a 2D face reenactment method [55] and two 3D avatar synthesis methods [24, 31]. Besides, we also compare with an optimization-based baseline Next3D-PTI, which incorporates an animatable 3D GAN [40] and pivotal tuning inversion [37].

Evaluation Metrics. We evaluate reconstruction and reenactment quality using peak signal-to-noise ratio (PSNR), Learned Perceptual Image Patch Similarity (LPIPS) [58] for synthetic quality, cosine similarity (CSIM) [10] for identity preservation, and average keypoint distance (AKD) using a SOTA off-the-shelf facial landmarks detector¹ for reenactment quality.

4.2. Comparisons

4.2.1 One-shot Avatar Reconstruction

We evaluate same-identity and cross-identity reenactment using various methods. For self-reenactment, the first frame of HDTF test videos served as the source, with the next 500 frames as the driving video. In cross-identity cases, the first 200 frames of one HDTF clip compose the driving video, and the first frame of other videos as source images. Besides, following [55], We also transfer motions from videos to CelebA-HQ monocular images [22], using test videos from HDTF and VFHQ, creating 100,000 synthesized images from 1000 CelebA-HQ images and 25 video clips². Without ground truth for cross-reenactment, we relied on CSIM and AKD metrics for evaluation.

Tab.1 presents quantitative evaluations on the HDTF and CelebA-HQ datasets, while Fig. 3 showcases the qualitative results of cross-identity reenactment on the CelebA-HQ dataset. Our method shows superior generalization on these unseen datasets, surpassing others in identity preservation, appearance recovery, and expression control. It outperforms baselines in capturing fine details such as hair

¹<https://github.com/google/mediapipe>

²In addition to 19 videos from the testing split of HDTF, we also select 6 videos with rich expression changes from VFHQ as supplements.

Method	Same-ID on HDTF					Cross-ID on HDTF		Cross-ID on CelebA	
	PSNR \uparrow	L1 \downarrow	LPIPS \downarrow	CSIM \uparrow	AKD \downarrow	CSIM \uparrow	AKD \downarrow	CSIM \uparrow	AKD \downarrow
Ours	23.27	0.029	0.111	0.873	0.018	0.759	0.041	0.755	0.069
OTAvatar	22.85	0.035	0.133	0.794	0.136	0.669	0.420	0.569	2.050
Next3D-PTI	22.05	0.038	0.128	0.850	0.312	0.651	0.577	0.648	0.788
StyleHEAT	22.32	0.036	0.130	0.827	0.109	0.710	0.216	0.604	0.348
ROME	22.91	0.034	0.127	0.832	0.120	0.722	0.239	0.682	0.299

Table 1. Quantitative Evaluation for one-shot avatar reconstruction and animation.

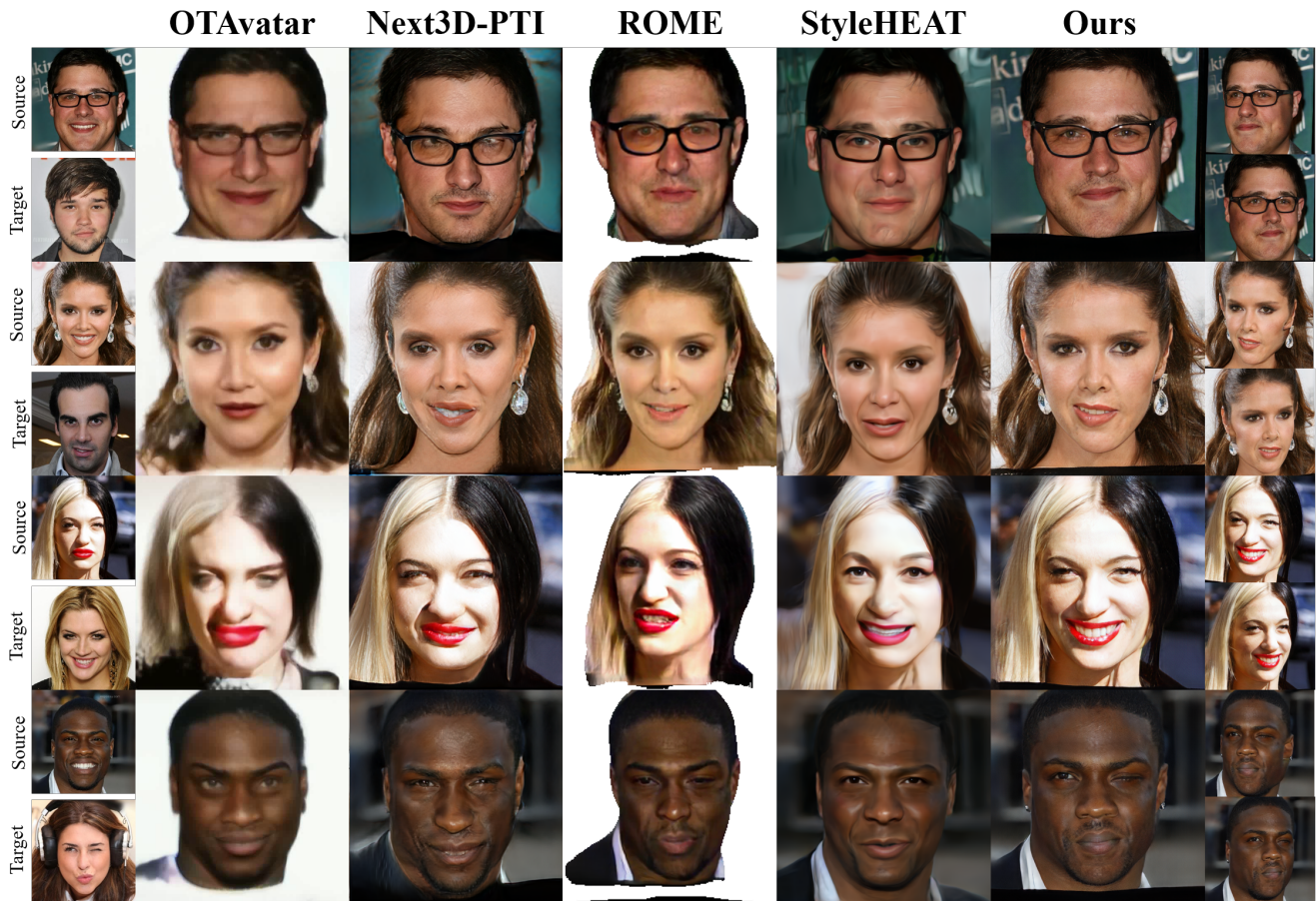


Figure 3. Qualitative comparison on the CelebA-HQ for one-shot avatar reconstruction. The results demonstrate the superior performance of our method in terms of realistic appearance recovery and fine-grained expression control.

strands and earrings. Additionally, it also excels in expression transfer, offering precise control over nuanced expressions like asymmetrical mouth movements and eye gazes. In comparison, ROME [24] fails to capture high-frequency details, StyleHeat [55] struggles with inner mouth synthesis, and OTAvatar [31] is unable to generate photo-realistic facial avatars with compact latent vector encoding. Although Next3D-PTI can reconstruct avatars with test-time optimization, it falls short in precise expression control.

4.2.2 Few-shot Avatar Reconstruction

Without readily available benchmarks for few-shot avatar reconstruction, we adapt one-shot methods, both our method and OTAvatar [31], to accommodate multiple source images. This adaptation involves reconstructing canonical features from each source image, followed by averaging these features to derive a canonical space representation. Specifically, for OTAvatar, we compute the mean identity latent code. For our one-shot method, we averaged the feature maps F_{tex} and F_{tri} in both two canonical spaces.

	2 source frames					4 source frames				
	PSNR \uparrow	LPIPS \downarrow	AKD \downarrow	CSIM \uparrow	Time(s)	PSNR \uparrow	LPIPS \downarrow	AKD \downarrow	CSIM \uparrow	Time(s)
Ours	23.39	0.170	0.024	0.867	0.20	23.58	0.162	0.022	0.873	0.32
OTAvatar	17.39	0.281	0.696	0.736	50	17.76	0.276	0.614	0.721	100
Ours-OS	22.40	0.202	0.029	0.846	0.36	22.78	0.202	0.026	0.839	0.71
Next3D-PTI	20.23	0.199	0.637	0.821	150	20.74	0.1771	0.287	0.845	150

Table 2. Quantitative Evaluation on VFHQ-Test using multiple source images.

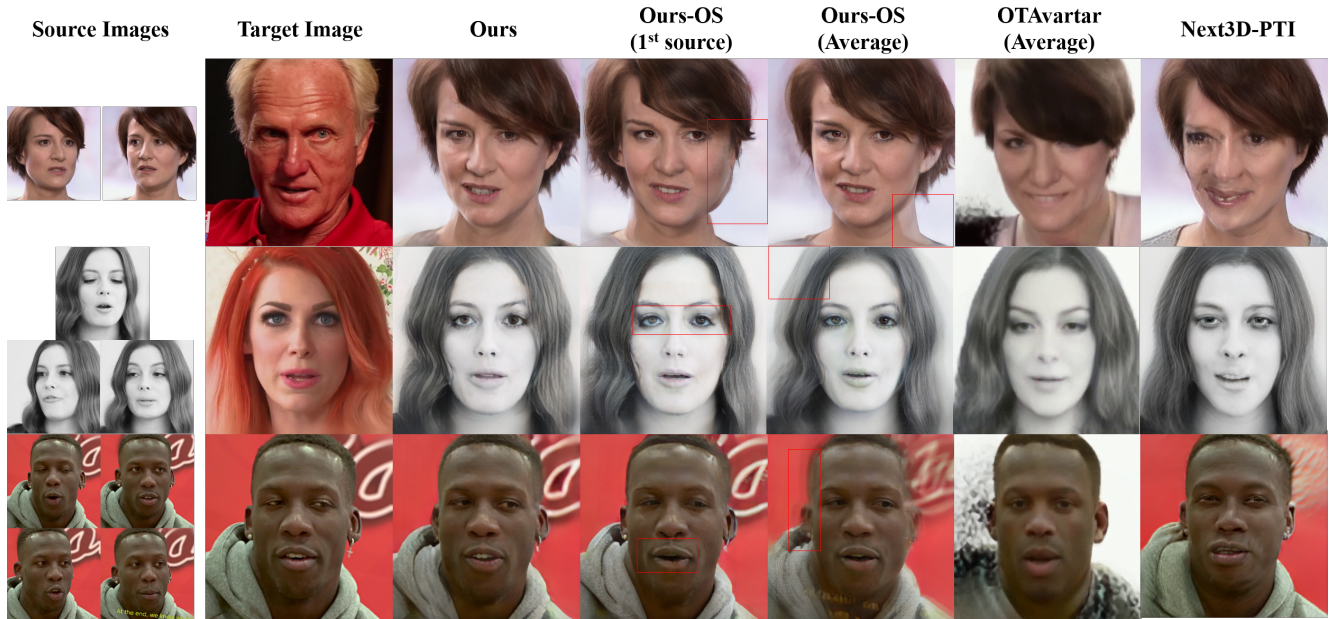


Figure 4. Qualitative comparison on the VFHQ-Test for few-shot avatar reconstruction and animation. Our method integrates multi-frame observations to improve shape reconstruction and texture recovery, as well as retaining high fidelity.

Due to the diverse expressions and poses in VFHQ [53], we evaluate using a test dataset of 100 VFHQ videos, each with 300 frames, excluding training set subjects. We sample input frames evenly from the initial 200 frames and use the last 100 frames for performance evaluation.

Tab. 2 and Fig. 2 display the results obtained with varying numbers of input frames. Our incremental GAN inversion framework, in comparison to the one-shot inversion using only the first frame, adeptly integrates multi-frame data to fill in information gaps present in a single image, thus enhancing the geometry and texture details. For example, this is evident in the improved depiction of hair shape (row 1, Fig. 2), pupil color (row 2), and teeth refinement (row 3). Adapted one-shot methods, despite warping features from each source image to the canonical space, suffer from the misalignment of these inverted features, leading to blurry and inaccurate outputs. Our approach mitigates these issues, thanks to our RNN-based temporal aggregation network’s effectiveness in merging sequential features, which is critical for achieving realistic detail recovery, as seen in

the hair strands in Fig. 1.

For efficiency, OTAvatar[31] and Next3D-PTI require lengthy optimization for novel identities. In contrast, our learning-based solution achieves rapid avatar reconstruction within one second, with the time cost increasing only marginally with the number of input frames.

4.3. Ablation Studies

4.3.1 Recurrent mechanism for temporal aggregation

To evaluate our recurrent mechanism, we establish a fixed-window baseline termed “ConvFusion”, which replaces each GRU block with a convolutional block to compress temporal features. Due to its fixed input capacity, “ConvFusion” averages the inverted canonical features when handling longer sequences.

Fig. 5 demonstrates the use of an 8-frame video clip to mimic an online stream. Our method shows incremental improvements in the reconstructed shape and appearance with the increase in frames. In contrast, “ConvFusion” lacks the ability to discern which information to retain or discard, and

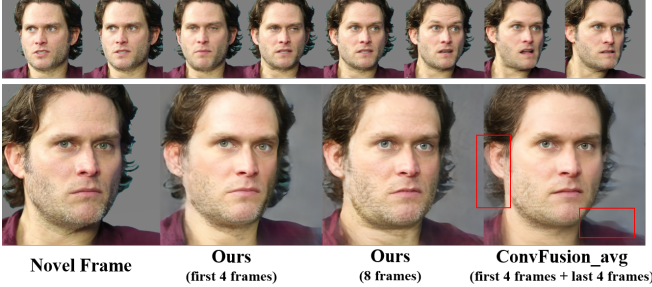


Figure 5. With a continuous input video stream, our method incrementally refines facial shape and texture details, in contrast to the fixed-window baseline “ConvFusion_avg”, which tends to produce blurry outcomes.

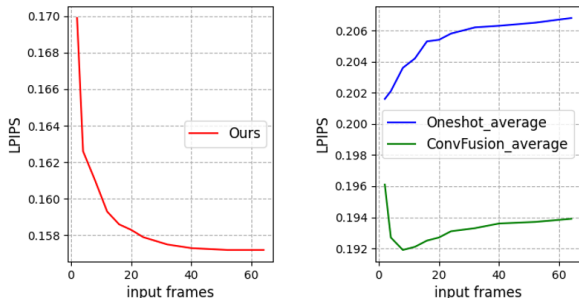


Figure 6. LPIPS over the number of input frames on VFHQ-test. With longer sequences, our method shows improving and converging metrics, affirming its proficiency in long-term temporal aggregation, unlike fixed-window baselines that degrade as source image count consistently increases.

a simple averaging strategy results in a blurred feature space and inferior rendering results.

A similar pattern emerges in Fig. 6, where we simulate processing offline video sequences, assessing performance against the number of input frames. On the VFHQ-test, with denser sampling in the first 200-frame sequence, The error of “ConvFusion” initially decreases but then increases after the frame count exceeds its fixed-window size. Conversely, our recurrent framework’s performance improves incrementally with additional frames and then remains stable.

4.3.2 Encoder design for canonical space inversion

Prediction of tri-plane SFT parameters. We introduce a baseline approach that utilizes E_{tri} to directly predict feature offsets. As illustrated in Fig. 7 and Tab. 3, our approach of predicting SFT parameters for modulating G_{sta} lessens the impact of the initial coarse facial avatar, thereby reducing artifacts and improving fidelity.

Neural Texture Encoder. We set a baseline with posed images as inputs to E_{tex} . As shown in Fig. 7 and Tab. 3, our

	LPIPS↓	PSNR↑	CSIM↑	FID↓
Ours	0.180	25.34	0.933	23.25
wo both Enc	0.393	17.67	0.809	26.42
wo NT Enc	0.201	24.35	0.910	28.23
E_{tri} offsets	0.244	21.97	0.889	34.36

Table 3. Ablation studies on CelebA-HQ for portrait reconstruction, to validate the effectiveness of our encoder design.

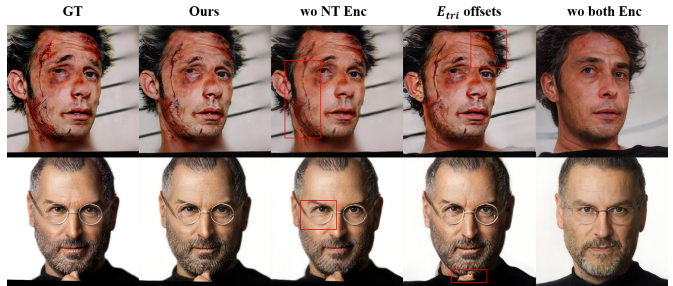


Figure 7. Qualitative ablation study results on the encoder design for canonical space inversion. Zoom in for the best view.

neural texture encoder, designed to prioritize pixel-aligned image-to-image translation on the UV parameterization, is vital for faithful facial detail recovery.

5. Discussion and Conclusion

Limitation. Dependent on a parametric model to control facial expressions, our method struggles with extreme expressions beyond the model’s capability, like frowning and sticking tongue out. Additionally, synthesizing stable, clear dynamic lower teeth remains challenging. Future advancements in more robust facial models capable of tracking these aspects are likely to enhance the performance.

Potential Social Impact. Considering our method can reconstruct a vivid personalized head character using a single image in less than one second, it may be used for generating “deepfakes”, which should be addressed carefully before deploying the technology.

Conclusion. We present *Incremental 3D GAN Inversion*, a feedforward pipeline for generalized 3D head avatar creation, supporting one or multiple image inputs. We employ an animatable 3D GAN prior and a novel UV-aligned neural texture encoder for detail recovery and ConvGRU-based recurrent networks for effective temporal fusing of streaming data. Experiments have demonstrated our method outperforms the state-of-the-art approaches in both one-shot and few-shot avatar animation tasks. We believe our method with a flexible number of input frames will make progress for the GAN inversion methods.

References

- [1] Rameen Abdal, Yipeng Qin, and Peter Wonka. Image2stylegan: How to embed images into the stylegan latent space? In *ICCV*, 2019. 2
- [2] Yuval Alaluf, Or Patashnik, and Daniel Cohen-Or. Restyle: A residual-based stylegan encoder via iterative refinement. In *ICCV*, 2021. 2
- [3] ShahRukh Athar, Zexiang Xu, Kalyan Sunkavalli, Eli Shechtman, and Zhixin Shu. Rignerf: Fully controllable neural 3d portraits. In *CVPR*, 2022. 1, 3
- [4] Yunpeng Bai, Yanbo Fan, Xuan Wang, Yong Zhang, Jingxiang Sun, Chun Yuan, and Ying Shan. High-fidelity facial avatar reconstruction from monocular video with generative priors. In *Proceedings of the IEEE/CVF Conference on Computer Vision and Pattern Recognition*, pages 4541–4551, 2023. 2, 3
- [5] Nicolas Ballas, Li Yao, Chris Pal, and Aaron Courville. Delving deeper into convolutional networks for learning video representations. *arXiv preprint arXiv:1511.06432*, 2015. 2, 5
- [6] Ananta R Bhattarai, Matthias Nießner, and Artem Sevastopolsky. Triplanenet: An encoder for eg3d inversion. *arXiv preprint arXiv:2303.13497*, 2023. 3, 2
- [7] Volker Blanz and Thomas Vetter. A morphable model for the synthesis of 3d faces. In *Proceedings of the 26th Annual Conference on Computer Graphics and Interactive Techniques*, page 187–194, USA, 1999. ACM Press/Addison-Wesley Publishing Co. 2, 3
- [8] Eric R. Chan, Connor Z. Lin, Matthew A. Chan, Koki Nagano, Boxiao Pan, Shalini De Mello, Orazio Gallo, Leonidas Guibas, Jonathan Tremblay, Sameh Khamis, Tero Karras, and Gordon Wetzstein. Efficient geometry-aware 3D generative adversarial networks. In *CVPR*, 2022. 1
- [9] Hang Dai, Nick Pears, William Smith, and Christian Duncan. Statistical modeling of craniofacial shape and texture. *International Journal of Computer Vision*, 128(2):547–571, 2020. 3
- [10] Jiankang Deng, Jia Guo, Xue Niannan, and Stefanos Zafeiriou. Arcface: Additive angular margin loss for deep face recognition. In *CVPR*, 2019. 5, 1, 2
- [11] Yu Deng, Jiaolong Yang, Dong Chen, Fang Wen, and Tong Xin. Disentangled and controllable face image generation via 3d imitative-contrastive learning. In *Proceedings of the IEEE Conference on Computer Vision and Pattern Recognition (CVPR)*, 2020. 1, 2, 3
- [12] Tan M. Dinh, Anh Tuan Tran, Rang Nguyen, and Binh-Son Hua. Hyperinverter: Improving stylegan inversion via hypernetwork. In *CVPR*, 2022. 2
- [13] Michail Christos Doukas, Stefanos Zafeiriou, and Viktoriia Sharmanska. Headgan: One-shot neural head synthesis and editing. In *Proceedings of the IEEE/CVF International Conference on Computer Vision*, pages 14398–14407, 2021. 1, 2, 3
- [14] Qianli Feng, Viraj Shah, Raghudeep Gadde, Pietro Perona, and Aleix Martinez. Near perfect gan inversion. *arXiv preprint arXiv:2202.11833*, 2022. 2
- [15] Ohad Fried, Ayush Tewari, Michael Zollhöfer, Adam Finkelstein, Eli Shechtman, Dan B Goldman, Kyle Genova, Zeyu Jin, Christian Theobalt, and Maneesh Agrawala. Text-based editing of talking-head video. *ACM Transactions on Graphics (TOG)*, 38(4):1–14, 2019. 3
- [16] Guy Gafni, Justus Thies, Michael Zollhofer, and Matthias Nießner. Dynamic neural radiance fields for monocular 4d facial avatar reconstruction. In *Proceedings of the IEEE/CVF Conference on Computer Vision and Pattern Recognition*, pages 8649–8658, 2021. 1, 3
- [17] Baris Gecer, Binod Bhattarai, Josef Kittler, and Tae-Kyun Kim. Semi-supervised adversarial learning to generate photorealistic face images of new identities from 3d morphable model. In *Proceedings of the European conference on computer vision (ECCV)*, pages 217–234, 2018. 3
- [18] Baris Gecer, Stylianos Ploumpis, Irene Kotsia, and Stefanos Zafeiriou. Ganfit: Generative adversarial network fitting for high fidelity 3d face reconstruction. In *Proceedings of the IEEE/CVF conference on computer vision and pattern recognition*, pages 1155–1164, 2019. 3
- [19] Philip-William Grassal, Malte Prinzler, Titus Leistner, Carsten Rother, Matthias Nießner, and Justus Thies. Neural head avatars from monocular rgb videos. In *Proceedings of the IEEE/CVF Conference on Computer Vision and Pattern Recognition*, pages 18653–18664, 2022. 1, 3
- [20] Jiatao Gu, Qingzhe Gao, Shuangfei Zhai, Baoquan Chen, Lingjie Liu, and Josh Susskind. Learning controllable 3d diffusion models from single-view images. *arXiv preprint arXiv:2304.06700*, 2023. 3
- [21] Angjoo Kanazawa, Shubham Tulsiani, Alexei A. Efros, and Jitendra Malik. Learning category-specific mesh reconstruction from image collections. In *ECCV*, 2018. 3
- [22] Tero Karras, Timo Aila, Samuli Laine, and Jaakko Lehtinen. Progressive growing of GANs for improved quality, stability, and variation. In *ICLR*, 2018. 5
- [23] Tero Karras, Samuli Laine, Miika Aittala, Janne Hellsten, Jaakko Lehtinen, and Timo Aila. Analyzing and improving the image quality of StyleGAN. In *CVPR*, 2020. 2, 1
- [24] Taras Khakhulin, Vanessa Sklyarova, Victor Lempitsky, and Egor Zakharov. Realistic one-shot mesh-based head avatars. In *ECCV*, 2022. 5, 6
- [25] Hyeonwoo Kim, Pablo Garrido, Ayush Tewari, Weipeng Xu, Justus Thies, Matthias Niessner, Patrick Pérez, Christian Richardt, Michael Zollhöfer, and Christian Theobalt. Deep video portraits. *ACM Transactions on Graphics (TOG)*, 37(4):1–14, 2018. 3
- [26] Jaehoon Ko, Kyusun Cho, Daewon Choi, Kwangrok Ryoo, and Seungryong Kim. 3d gan inversion with pose optimization. In *WACV*, 2023. 2
- [27] Tianye Li, Timo Bolkart, Michael J. Black, Hao Li, and Javier Romero. Learning a model of facial shape and expression from 4D scans. *ACM Transactions on Graphics, (Proc. SIGGRAPH Asia)*, 36(6):194:1–194:17, 2017. 4
- [28] Tianye Li, Timo Bolkart, Michael J Black, Hao Li, and Javier Romero. Learning a model of facial shape and expression from 4d scans. *ACM Trans. Graph.*, 36(6):194–1, 2017. 3

- [29] Xueting Li, Shalini De Mello, Sifei Liu, Koki Nagano, Umar Iqbal, and Jan Kautz. Generalizable one-shot neural head avatar. *arXiv preprint arXiv:2306.08768*, 2023. [2](#), [3](#)
- [30] C.Z. Lin, D.B. Lindell, E.R. Chan, and G. Wetzstein. 3d gan inversion for controllable portrait image animation. In *ECCV Workshop on Learning to Generate 3D Shapes and Scenes*, 2022. [2](#)
- [31] Zhiyuan Ma, Xiangyu Zhu, Guo-Jun Qi, Zhen Lei, and Lei Zhang. Otavatar: One-shot talking face avatar with controllable tri-plane rendering. In *Proceedings of the IEEE/CVF Conference on Computer Vision and Pattern Recognition*, pages 16901–16910, 2023. [2](#), [3](#), [5](#), [6](#), [7](#)
- [32] Ben Mildenhall, Pratul P Srinivasan, Matthew Tancik, Jonathan T Barron, Ravi Ramamoorthi, and Ren Ng. NeRF: Representing scenes as neural radiance fields for view synthesis. In *ECCV*, 2020. [3](#)
- [33] Songyou Peng, Michael Niemeyer, Lars Mescheder, Marc Pollefeys, and Andreas Geiger. Convolutional occupancy networks. In *ECCV*, 2020. [3](#)
- [34] Stylianos Ploumpis, Evangelos Ververas, Eimear O’Sullivan, Stylianos Moschoglou, Haoyang Wang, Nick Pears, William AP Smith, Baris Gecer, and Stefanos Zafeiriou. Towards a complete 3d morphable model of the human head. *IEEE transactions on pattern analysis and machine intelligence*, 43(11):4142–4160, 2020. [3](#)
- [35] Yurui Ren, Ge Li, Yuanqi Chen, Thomas H Li, and Shan Liu. Pirenderer: Controllable portrait image generation via semantic neural rendering. In *Proceedings of the IEEE/CVF International Conference on Computer Vision*, pages 13759–13768, 2021. [1](#), [2](#), [3](#)
- [36] Elad Richardson, Yuval Alaluf, Or Patashnik, Yotam Nitzan, Yaniv Azar, Stav Shapiro, and Daniel Cohen-Or. Encoding in style: a stylegan encoder for image-to-image translation. In *CVPR*, 2021. [2](#), [5](#)
- [37] Daniel Roich, Ron Mokady, Amit H Bermano, and Daniel Cohen-Or. Pivotal tuning for latent-based editing of real images. *arXiv preprint arXiv:2106.05744*, 2021. [2](#), [5](#)
- [38] Vincent Sitzmann, Justus Thies, Felix Heide, Matthias Nießner, Gordon Wetzstein, and Michael Zollhöfer. DeepVoxels: Learning persistent 3D feature embeddings. In *CVPR*, 2019. [3](#)
- [39] Jingxiang Sun, Xuan Wang, Yichun Shi, Lizhen Wang, Jue Wang, and Yebin Liu. Ide-3d: Interactive disentangled editing for high-resolution 3d-aware portrait synthesis. *SIGGRAPH ASIA*, 2022. [2](#)
- [40] Jingxiang Sun, Xuan Wang, Lizhen Wang, Xiaoyu Li, Yong Zhang, Hongwen Zhang, and Yebin Liu. Next3d: Generative neural texture rasterization for 3d-aware head avatars. In *Proceedings of the IEEE/CVF Conference on Computer Vision and Pattern Recognition*, pages 20991–21002, 2023. [2](#), [3](#), [5](#), [1](#)
- [41] Junshu Tang, Bo Zhang, Binxin Yang, Ting Zhang, Dong Chen, Lizhuang Ma, and Fang Wen. 3dfaceshop: Explicitly controllable 3d-aware portrait generation. *IEEE Transactions on Visualization and Computer Graphics*, 2023. [2](#)
- [42] Ayush Tewari, Mohamed Elgharib, Gaurav Bharaj, Florian Bernard, Hans-Peter Seidel, Patrick Pérez, Michael Zollhofer, and Christian Theobalt. Stylerig: Rigging stylegan for 3d control over portrait images. In *Proceedings of the IEEE Conference on Computer Vision and Pattern Recognition (CVPR)*, 2020. [3](#)
- [43] Justus Thies, Michael Zollhofer, Marc Stamminger, Christian Theobalt, and Matthias Nießner. Face2face: Real-time face capture and reenactment of rgb videos. In *Proceedings of the IEEE conference on computer vision and pattern recognition*, pages 2387–2395, 2016. [3](#)
- [44] Justus Thies, Michael Zollhöfer, and Matthias Nießner. Deferred neural rendering: Image synthesis using neural textures. *ACM Transactions on Graphics (TOG)*, 38(4):1–12, 2019. [3](#)
- [45] Omer Tov, Yuval Alaluf, Yotam Nitzan, Or Patashnik, and Daniel Cohen-Or. Designing an encoder for stylegan image manipulation. *SIGGRAPH*, 2021. [2](#), [5](#), [1](#)
- [46] Alex Trevithick, Matthew Chan, Michael Stengel, Eric R. Chan, Chao Liu, Zhiding Yu, Sameh Khamis, Manmohan Chandraker, Ravi Ramamoorthi, and Koki Nagano. Real-time radiance fields for single-image portrait view synthesis. In *ACM Transactions on Graphics (SIGGRAPH)*, 2023. [3](#), [5](#), [1](#)
- [47] Lizhen Wang, Zhiyua Chen, Tao Yu, Chenguang Ma, Liang Li, and Yebin Liu. Faceverse: a fine-grained and detail-controllable 3d face morphable model from a hybrid dataset. In *IEEE Conference on Computer Vision and Pattern Recognition (CVPR2022)*, 2022. [3](#), [4](#)
- [48] Lizhen Wang, Xiaochen Zhao, Jingxiang Sun, Yuxiang Zhang, Hongwen Zhang, Tao Yu, and Yebin Liu. Styleavatar: Real-time photo-realistic portrait avatar from a single video. *arXiv preprint arXiv:2305.00942*, 2023. [1](#), [2](#), [3](#)
- [49] Tengfei Wang, Yong Zhang, Yanbo Fan, Jue Wang, and Qifeng Chen. High-fidelity gan inversion for image attribute editing. In *CVPR*, 2022. [2](#)
- [50] Xintao Wang, Yu Li, Honglun Zhang, and Ying Shan. Towards real-world blind face restoration with generative facial prior. In *The IEEE Conference on Computer Vision and Pattern Recognition (CVPR)*, 2021. [5](#)
- [51] Yue Wu, Yu Deng, Jiaolong Yang, Fangyun Wei, Qifeng Chen, and Xin Tong. Anifacegan: Animatable 3d-aware face image generation for video avatars. *Advances in Neural Information Processing Systems*, 35:36188–36201, 2022. [2](#)
- [52] Jiaxin Xie, Hao Ouyang, Jingtian Piao, Chenyang Lei, and Qifeng Chen. High-fidelity 3d gan inversion by pseudo-multi-view optimization. In *Proceedings of the IEEE/CVF Conference on Computer Vision and Pattern Recognition*, pages 321–331, 2023. [2](#)
- [53] Liangbin Xie, Xintao Wang, Honglun Zhang, Chao Dong, and Ying Shan. Vfhq: A high-quality dataset and benchmark for video face super-resolution. In *Proceedings of the IEEE/CVF Conference on Computer Vision and Pattern Recognition*, pages 657–666, 2022. [7](#), [2](#)
- [54] Sicheng Xu, Jiaolong Yang, Dong Chen, Fang Wen, Yu Deng, Yunde Jia, and Xin Tong. Deep 3d portrait from a single image. In *Proceedings of the IEEE/CVF Conference on Computer Vision and Pattern Recognition*, pages 7710–7720, 2020. [3](#)
- [55] Fei Yin, Yong Zhang, Xiaodong Cun, Mingdeng Cao, Yanbo Fan, Xuan Wang, Qingyan Bai, Baoyuan Wu, Jue Wang,

- and Yujiu Yang. Styleheat: One-shot high-resolution editable talking face generation via pre-trained stylegan. In *European conference on computer vision*, pages 85–101. Springer, 2022. [5](#), [6](#)
- [56] Wangbo Yu, Yanbo Fan, Yong Zhang, Xuan Wang, Fei Yin, Yunpeng Bai, Yan-Pei Cao, Ying Shan, Yang Wu, Zhongqian Sun, et al. Nofa: Nerf-based one-shot facial avatar reconstruction. In *ACM SIGGRAPH 2023 Conference Proceedings*, pages 1–12, 2023. [3](#)
- [57] Jingbo Zhang, Xiaoyu Li, Ziyu Wan, Can Wang, and Jing Liao. Fdnerf: Few-shot dynamic neural radiance fields for face reconstruction and expression editing. *arXiv preprint arXiv:2208.05751*, 2022. [1](#), [3](#)
- [58] Richard Zhang, Phillip Isola, Alexei A Efros, Eli Shechtman, and Oliver Wang. The unreasonable effectiveness of deep features as a perceptual metric. In *CVPR*, 2018. [5](#), [1](#)
- [59] Yufeng Zheng, Victoria Fernández Abrevaya, Marcel C Bühler, Xu Chen, Michael J Black, and Otmar Hilliges. Im avatar: Implicit morphable head avatars from videos. In *Proceedings of the IEEE/CVF Conference on Computer Vision and Pattern Recognition*, pages 13545–13555, 2022. [1](#), [3](#)
- [60] Yufeng Zheng, Wang Yifan, Gordon Wetzstein, Michael J Black, and Otmar Hilliges. Pointavatar: Deformable point-based head avatars from videos. In *Proceedings of the IEEE/CVF Conference on Computer Vision and Pattern Recognition*, pages 21057–21067, 2023. [1](#)

InvertAvatar: Incremental GAN Inversion for Generalized Head Avatars

Supplementary Material

6. Implementation Details

In this section, we’ll discuss the implementation details of each framework component, including training specifics and network architectures.

6.1. Training Animatable 3D GAN

We implement our 3D GAN framework on top of the official PyTorch implementation of Next3D [40], and we illustrate the differences in network architecture between ours and Next3D in Fig 8. Specifically, we rasterize neural texture feature maps at the resolutions of (32, 64, 128) for multi-scale conditions on G_{face} .

We adopt many hyperparameters and training strategies of EG3D [8] and Next3D [40] including blurred real images at the beginning, pose conditioned generator, density regularization, learning rates, and two-stage training. As for the deformation-aware discriminator, we replace the input synthetic rendering image with the landmarks counter map to force the generator to focus on the expression changes in the mouth and eyes region. During the training process, we follow Next3D and adopt the same loss terms. Specifically, we train the network on FFHQ [23], using the non-saturating GAN loss with R1 regularization and the density regularization proposed in EG3D. Based on the pretrained model of EG3D, we train our model at a neural rendering resolution of 64 on four 3090 GPUs with a batch size of 16 for roughly 2 days and gradually step the resolution up to 128 for additional 2 days.

6.2. Training Encoders

To promote inversion performance and minimize GPU memory usage during training, we adopt a three-stage training schedule, which separately trains the latent encoder E_{latent} , image encoders E_{tex} and E_{tri} in a one-shot setting, and temporal aggregation encoders $E_{tex.rec}$ and $E_{tri.rec}$ in a multi-shot setting.

6.2.1 Training E_{latent}

For training the latent encoder E_{latent} , we employ pixel-wise L_1 loss, perceptual loss L_{lpips} [58], and identity similarity loss L_{ID} [10]. Besides, we follow [45] and set a latent discriminator D_W to discriminate between real samples from the W space and the latent codes predicted by the encoder. The encoder is trained in an adversarial scheme and the total loss can be written as :

$$L_{stage1} = L_1 + \lambda_{lpips}L_{lpips} + \lambda_{id}L_{ID} + L_{adv}^{D_W} + L_{adv}^{E_{latent}} \quad (2)$$

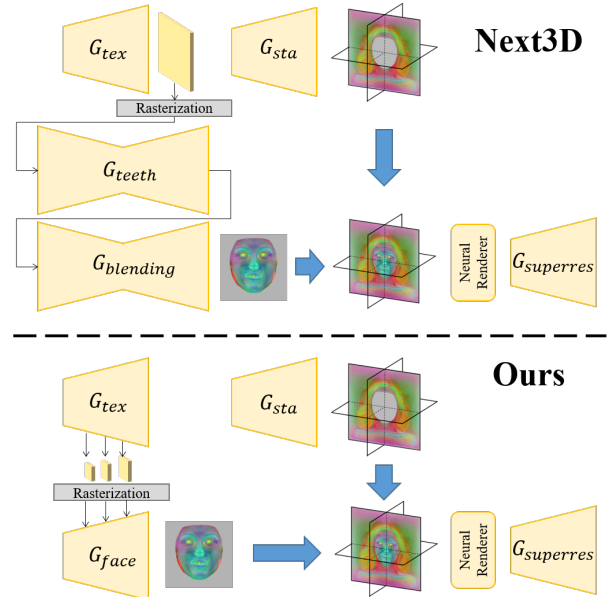


Figure 8. Comparison of the network architecture of Next3D against ours. Our more memory-friendly and compact representation allows for efficient training at a neural rendering resolution of 128^2 , which significantly improves view consistency.

where $\lambda_{lpips} = 0.5$, $\lambda_{id} = 0.25$. The learning rates for the encoder and latent discriminator are both $1e-4$. Based on the FFHQ dataset, the training is conducted on four 3090 GPUs with a batch size of 16 for 2 days.

6.2.2 Training E_{tri} and E_{tex}

In this stage, we fix the latent encoder E_{latent} and train both UNet-style networks E_{tri} and E_{tex} with image datasets. Besides the FFHQ dataset, we also utilize the synthetic data generated by the pretrained GAN to prompt multi-view consistent reconstruction.

Inspired by [46], leveraging synthetic data, we supervise the training with intermediate feature maps, including neural texture maps F_{tex} , tri-plane feature maps F_{tri} and neural rendering feature maps I_{raw} . Loss can be written as:

$$L_{stage2} = L_1 + \lambda_{lpips}L_{lpips} + \lambda_{tri}L_{tri} + \lambda_{tex}L_{tex} + \lambda_{raw}L_{raw} + \lambda_{adv}L_{adv} \quad (3)$$

where $\lambda_{lpips} = 1.0$, $\lambda_{tri} = 0.001$, $\lambda_{tex} = 0.001$, $\lambda_{raw} = 1.0$, $\lambda_{adv} = 0.1$. L_{tri} , L_{tex} , L_{raw} are the L1 losses that intuitively compare those quantities synthesized by our generative model and those created by our encoders. L_{adv} is the adversarial loss using a dual discriminator [8], which is

trained to differentiate between synthetic images sampled from GAN prior and the corresponding image reconstructed by the encoders. We remove the pose condition for the dual discriminator. On four 3090 GPUs with a batch size of 16, we first train both image encoders without the generative adversarial objective for about 4 days, and then add adversarial loss to finetune encoders for an additional day. We use a learning rate of 1e-4 for encoders and 1e-3 for the discriminator.

6.2.3 Training $E_{tri.rec}$ and $E_{tex.rec}$

Building upon pretrained E_{tri} and E_{tex} , $E_{tri.rec}$ and $E_{tex.rec}$ maintain fixed encoding backbone and only finetune their recurrent decoders. To learn to aggregate temporal information from monocular videos, we leverage 7500 real-world video clips from the VFHQ video dataset [53], each comprising 100 frames. However, since the image quality in the video dataset typically lags behind that of the GAN prior from the FFHQ dataset, training only with the VFHQ data causes blurry and degraded renderings. Hence during training, we simultaneously use the synthetic video data, which has random identity sampled from the GAN latent space, with poses and expressions sampled from the VFHQ video dataset. This additional synthetic data supplementation improves the quality of the generated images.

Due to GPU memory constraints, during training, the temporal aggregation networks $E_{tri.rec}$ and $E_{tex.rec}$ process a maximum of 4 frames at a time in the forward pass. This limitation can lead to overfitting on short sequences, hindering the efficient fusion of observations from longer sequences. Leveraging the RNN framework’s support for sequential inputs, we can initialize h_0 (Eq.1 in the main paper) to a non-zero state by cycling through the inputs during training. In practice, we input sequences of up to 32 frames³, randomly selecting 4 frames for rendering and loss calculation in each iteration. This strategy simulates the supervision over longer sequences to some extent, enhancing the ability of the update gates in GRU blocks to capture long-term dependencies and allowing the temporal aggregation networks to retain long-term temporal information.

We adopt the same loss terms and training strategy as in Sec 6.2.2. On eight 3090 GPUs with a batch size of 8, we train both encoders without the adversarial objective for about 3 days, and then finetune with adversarial loss for additional 24 hours.

6.3. Network Architecture

Latent Encoder To implement the latent encoder E_{latent} , we adopt the design of the e4e encoder [45] and employ IR-

SE-50 [10] pretrained model for the backbone network.

One-shot Image Encoders Adopting conventional U-Net architecture, E_{tri} and E_{tex} are designed based on TriplaneNet [6]. As both networks produce multi-resolution feature maps, we incorporate an extra MLP block at each layer to transform the output channels.

Temporal Aggregation Networks $E_{tex.rec}$ and $E_{tri.tex}$ are modified based on E_{tex} and E_{tri} . Specifically, we fix the down-sampling encoding part of the networks and replace the decoding parts with recurrent decoders by injecting a ConvGRU block at each layer.

7. More Qualitative Results

In Fig. 9, Fig. 10, Fig. 11, Fig. 13 and Fig. 12, we present more visualizations of cross-identity reenactment. Please also refer to our video for more clear comparisons.

³Longer input is allowed. But for 100-frame video clips in our training data, it’s dense enough to sample 32 frames

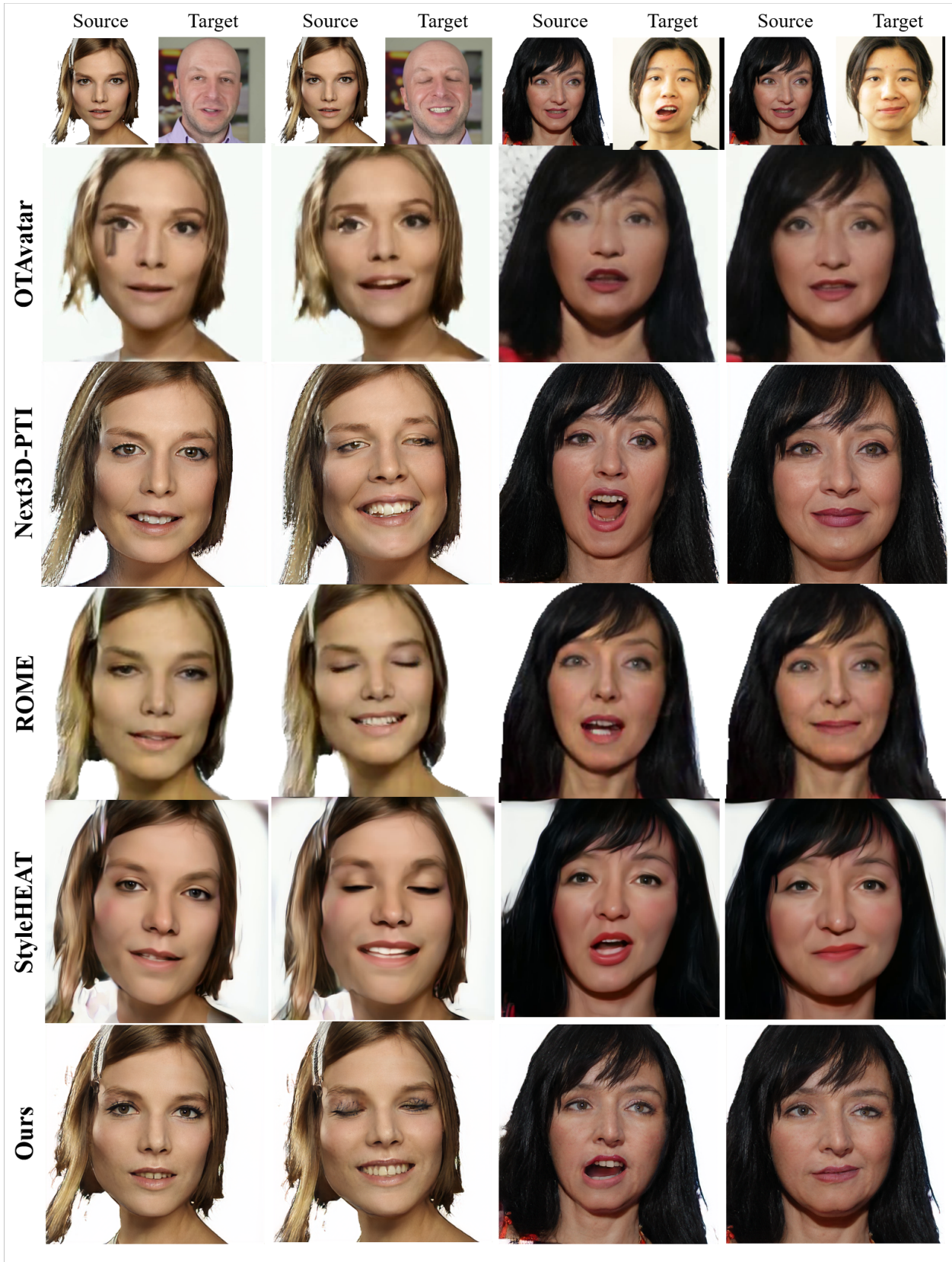


Figure 9. Cross-identity reenactment results of one-shot avatar reconstruction (part 1/3).



Figure 10. Cross-identity reenactment results of one-shot avatar reconstruction (part 2/3).

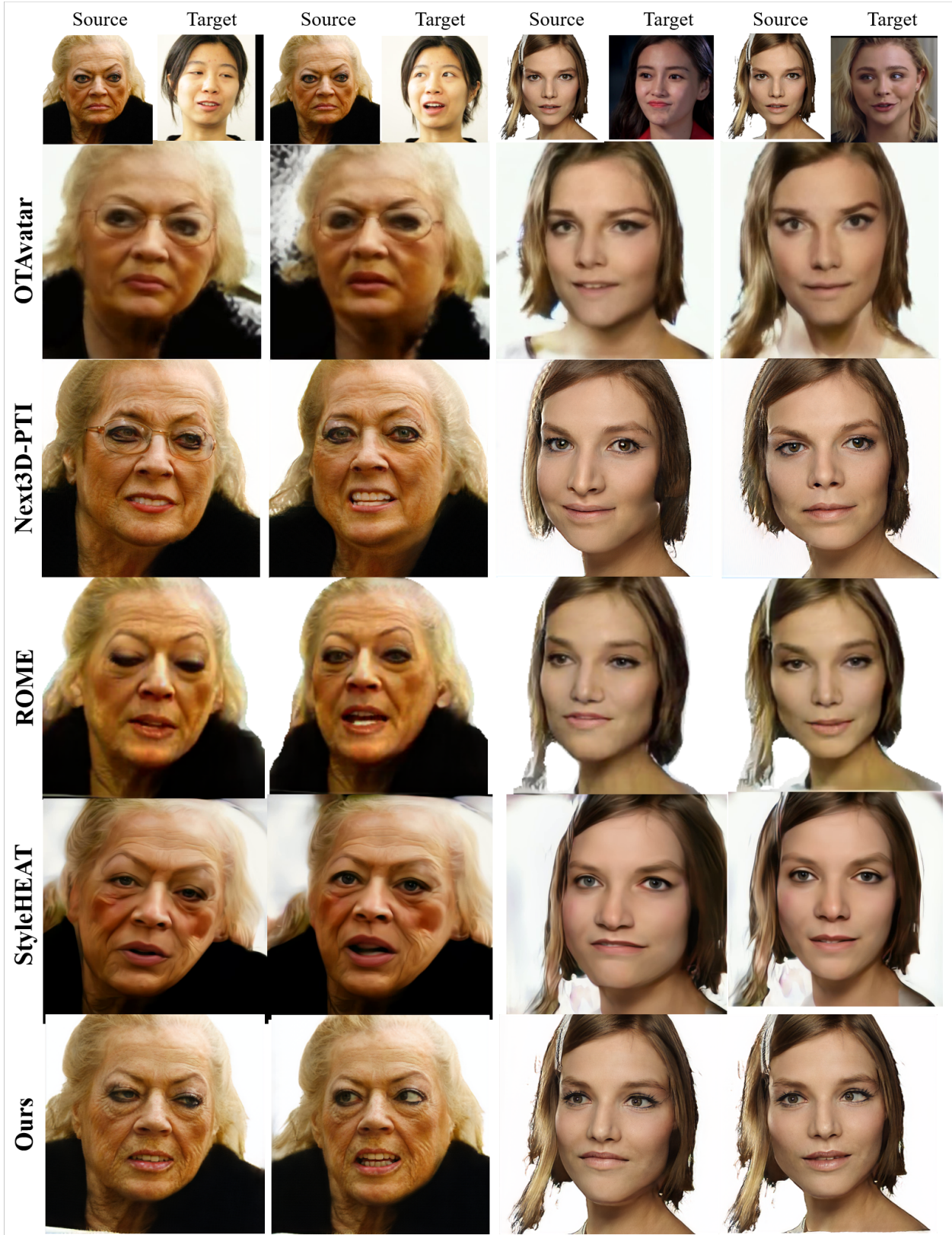


Figure 11. Cross-identity reenactment results of one-shot avatar reconstruction (part 3/3).



Figure 12. Cross-identity reenactment results of few-shot avatar reconstruction.

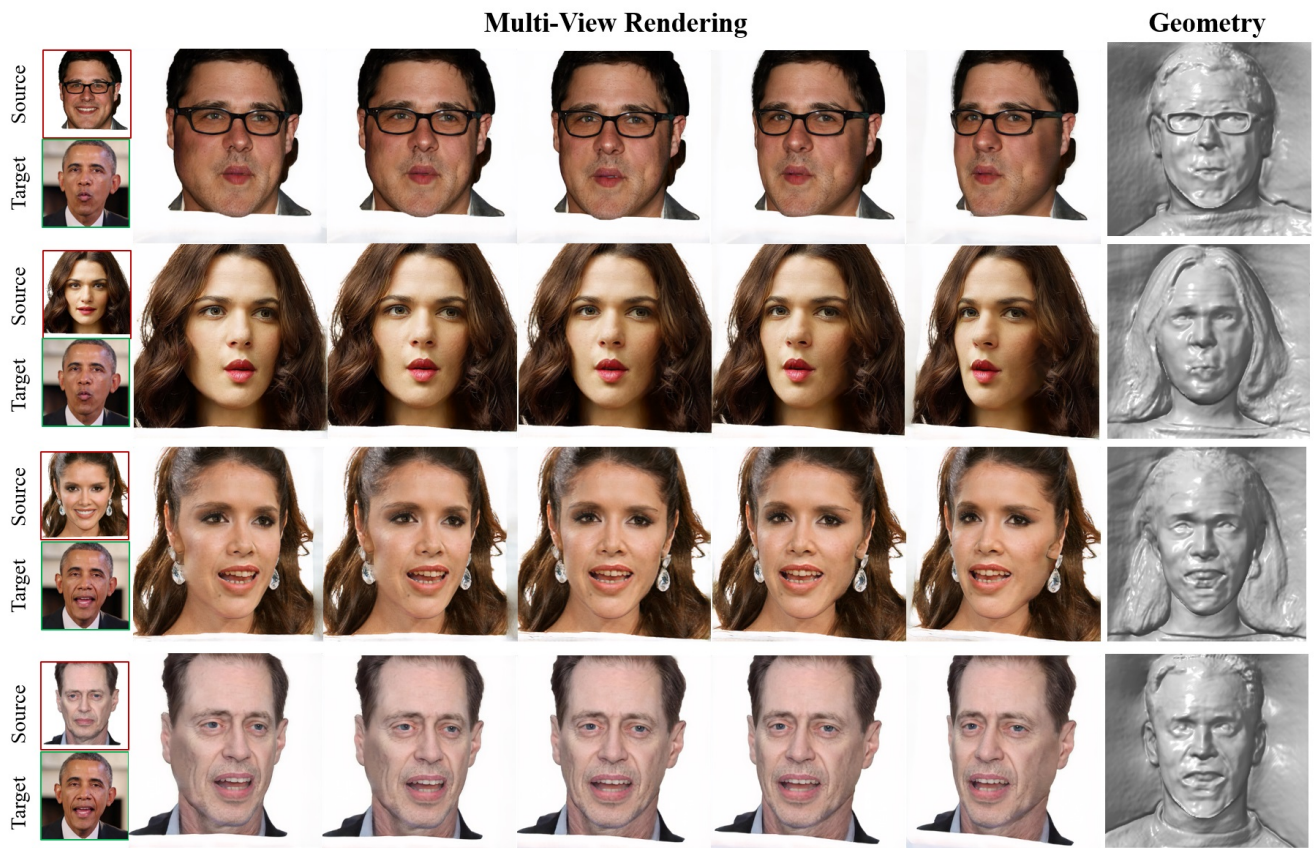


Figure 13. Cross-identity reenactment results of one-shot avatar reconstruction. We illustrate the multi-view rendering results and geometry.